Creep analysis of cementitious materials in seawater using a poro-chemo-mechanical model

Marinelle El-Khoury, Frederic Grondin, Benoit Hilloulin, Emmanuel Rozière, Rachid Cortas, Fadi Hage Chehade

Creep analysis of cementitious materials in seawater using a poro-chemo-mechanical model

Marinelle El-Khoury[1,2], Frédéric Grondin[1,*], Benoît Hilloulin[1], Emmanuel Rozière[1], Rachid Cortas[3], Fadi Hage Chehade[2]

[1] *Institut de Recherche en Génie Civil et Mécanique (GeM), UMR 6183, Centrale Nantes – Université de Nantes - CNRS, 1 rue de la Noë 44321 Nantes, France.*

[2] *Centre de Modélisation, Ecole Doctorale des Sciences et Technologie, Université Libanaise, Lebanon.*

[3] *Centre de Recherches Scientifiques en Ingénierie (CRSI), Université Libanaise, Beyrouth, Lebanon.*

[*] *Corresponding author.*

E-mail addresses: ***marinelle.el-khoury@ec-nantes.fr*** (M. El-Khoury); ***frederic.grondin@ec-nantes.fr*** (F. Grondin); ***benoit.hilloulin@ec-nantes.fr*** (B. Hilloulin); ***emmanuel.roziere@ec-nantes.fr*** (E. Roziere); ***rachid.cortas@ul.edu.lb*** (R. Cortas); ***fchehade@ul.edu.lb*** (F. Hage Chehade).

Abstract

With the rapid growth of the offshore engineering sector, studying the durability of offshore structures becomes primordial. Evaluating experimentally the coupling between mechanical and chemical degradation of the cement-based materials and structures is a challenging task because it requires tracking the evolution of the micro-mechanisms associated with the degradation in real time for long periods. To tackle this issue, a numerical approach is proposed, based on the micromechanics and the coupling between a creep-damage model and a chemical model at the microstructural scale. The seawater chemical effect on cement paste is simulated by considering the penetration fronts of the aggressive water and the attack by layers in the material. The aim of this study is to provide a tool for the rapid mechanical evaluation of the offshore structures and therefore a tool that can be used for the optimization and the development of durable marine constructions. The results highlight the competition between protective and damaged layers formed due to seawater attack, and that the global mechanical behaviour strongly depends on the chemically modified phases in the cement paste.

Key words

Micromechanics, poro-chemo-mechanical model, cementitious materials, offshore, creep, damage.

1. Introduction

The corrosion of steel reinforcement is a major issue for the durability of reinforced concrete (RC) structures exposed to seawater, especially for offshore concrete structures in marine environments. Previous studies have focused on the corrosion of steel due to the chloride ions diffusion [1–3] in harsh environments. Durability, safety, and sustainability of these infrastructures are critical especially in the transportation and in the oil and gas industry, where a failure can cause explosions, a huge gas leak in seawater, seawater contamination, loss of wildlife, and economical issues.

Nowadays, offshore constructions are growing rapidly especially in the energy and transportation sectors (wind farms, petroleum platforms and bridges, etc.). The use of concrete in these types of structures is frequent. Therefore, it is necessary to study the behaviour of concrete in marine environment.

The degradation of concrete structures in marine environments is induced by mechanical effects (creep, loss of strength and rigidity), chemical effects (seawater attack, external sulfate attack, chloride ions diffusion), and physical effects (temperature variation, freeze and thaw, erosion, etc.).

The diffusion-reaction phenomenon that takes place between the phases of cement paste and the seawater ions (chloride, sodium, magnesium and sulfate) is likely to induce the loss of particles from the concrete cover to reinforcement, the pollution of the marine environment, the degradation of the structure and the changes in the mechanical behaviour of the concrete structures. The diffusivity and other macroscopic mechanical properties depend on the mechanical and chemical damage in the microstructure. Therefore, coupling between mechanical and chemical degradation is likely to affect the durability of offshore structures.

The seawater attack caused by the ions diffusion into cement paste can create a competition between two opposing phenomena such as damage/expansion and the formation of protective layers [4,5]. This is due to the multiple interactions between the ions and the phases of cement

paste. Multiple works have focused on external sulfate attack [6–10] and chloride diffusion [11–13]. In the presence of Magnesium ions, an insoluble and possibly protective brucite layer is deposited on the surface of the concrete structure [14]. Brucite precipitation near the surface is commonly detected in magnesium-rich environments [15] as the output of base exchange reaction. The presence of CO_2 can lead to the calcium carbonate formation and its precipitation near the surface. Its stability is influenced by the water hardness and carbonate content, among other parameters. If stable, this calcium carbonate rich layer induces pore-blocking effect and mitigates leaching [16]. Seawater attack is significantly different from sulfate attacks at equivalent sulfate concentration [17]. In the presence of chloride ions, lower expansions and deteriorations are reported compared to sulfate attack [12,17]. The thickness of the sulfate enriched zone has actually been reported to be much lower than the depth affected by chloride diffusion [14]. The high chloride concentration of seawater actually induces the formation of Friedel's salt from AFm, which is thus less available to form ettringite known as expansive. Therefore, the formation of ettringite in a chloride-rich system would have a reduced tendency to generate expansion [18].

Few studies took into account the complexity of the combined chemical effects resulting from a combination of all ions present in marine environments and their consequences on the mechanical behaviour of cement-based materials. Therefore, when designing an offshore concrete structure it is primordial to consider the effect of all the ions present in seawater. The aim of this study is to create a multi-scale model coupling seawater attack with all its ions to the mechanical degradation of concrete structures.

It is necessary to start at the microscopic level and consider the diffusion and chemical interactions of each ion on the mechanical behaviour of the concrete structures. Performing this evaluation experimentally seems difficult because the evolution of the micro-mechanisms associated with the degradation in real time should be tracked for long periods of exposure at different scales. Multi-scale modelling, starting from the microscopic scale, seems relevant [19–21]. Therefore, a micromechanical model has been developed coupling the mechanical and chemical effects of seawater attack and the hydration process of cement paste.

The originality of this model lies in considering the combination of all ions present in seawater and evaluating their effects on the mechanical behaviour of the structure. It provides a tool for rapid mechanical assessment for offshore structures immerged in seawater for long periods.

Indeed, this chemo-mechanical model associates two codes: CemPP [22], simulating the coupling between hydration and chemical reactions at the scale of cement paste, and the finite element code Cast3M [23] simulating the creep-damage behaviour [24–27], loss or gain in the elastic properties consequently defining the mechanical constitutive law of the structure.

First, the coupling modelling approach is explained. Then, the hydration process and the seawater attack chemical reactions are presented and the model coupling between hydration and seawater attack is detailed. In the end, the creep damage model formulation is presented. Therefore, the coupling between chemical and mechanical effects is justified.

The results of the chemo-mechanical model are presented and analyzed at the microscopic and the mesoscopic levels.

2. The problem formulation

2.1. Coupling modelling procedure

Considering that the main chemical transformations occur in the offshore structures at the scale of the cement matrix, the study focuses on mortar and cement paste. Creep is due to the viscoelasticity of the cement paste restrained by sand particles and aggregates [20,28,29]. The chemical attack of the seawater mainly affects the cement paste and not aggregates, provided that aggregates are not sensitive to Alkali-Silica Reaction (ASR). In order to propose a behaviour law for the matrix of concrete, only mortars and cement pastes have been simulated. At the scale of cement paste, the cement hydration and the chemical reactions with seawater ions are modeled to obtain a microstructure of cement paste formed by a heterogeneous solid skeleton and pores. At the mortar scale, the material is formed by two continuous media: the cement paste, with average properties calculated from the lower scale, and the sand particles.

The proposed model presents the association of two codes: CemPP [22], for the simulation of the hydration and the chemical reactions at the scale of cement paste (**Hydration-Seawater attack model**) and the finite element code Cast3M [23] for the simulation of the creep-damage behaviour, loss or gain in the elastic properties consequently defining the mechanical strength of the structure (**Mechanical model**). The algorithm in Fig. 1 shows a graphical/visual summary on the multi-scale chemo mechanical model.

The originality of the model resides in its capacity of considering the heterogeneity of the material. The cement paste represents a heterogeneous material composed from multiple phases of anhydrous cement and hydration products, such as $C_3A, C_2S, C_3S, CH, CSH, ettringite, etc$. These phases and their properties are summarized in the Appendix A. The hydration of cement paste is modeled using CemPP v 0.2, based on the code CEMHYD3D v3 developed at NIST [30]. The digital volume is divided into 1µm^3 voxels in order to consider precisely the smallest hydration products as much as the capillary porosity. The size of the cement paste volume should be well defined to be representative of the material and the physics of phenomena. The cement properties (mineralogical composition and kinetics parameters) are input parameters.

Reactions due to seawater attack are considered in CemPP using a replacement mechanism of the reactant phases by the product phases (dedicated "Box replace pass"). The start and end of immersion time are defined as input parameters to the chemical model in order to trigger the chemical attack. Multiple 3D volumes of cement paste ($img_i \; at \; t_i$) are generated as output from the **hydration-seawater attack model**.

After generating the $img_i \; at \; t_i$, mechanical calculations are done at the same time t_i by considering the img_i as input data to the mechanical code (Cast3M).

Mechanical calculations are done on 2D sections extracted from the 3D volume generated from the chemical model (CemPP). Mechanical evaluation consists of determining, at t_i, the compressive strength, the tensile strength, Young's modulus and Poisson's coefficient via a damage model, and the creep compliance via a creep model.

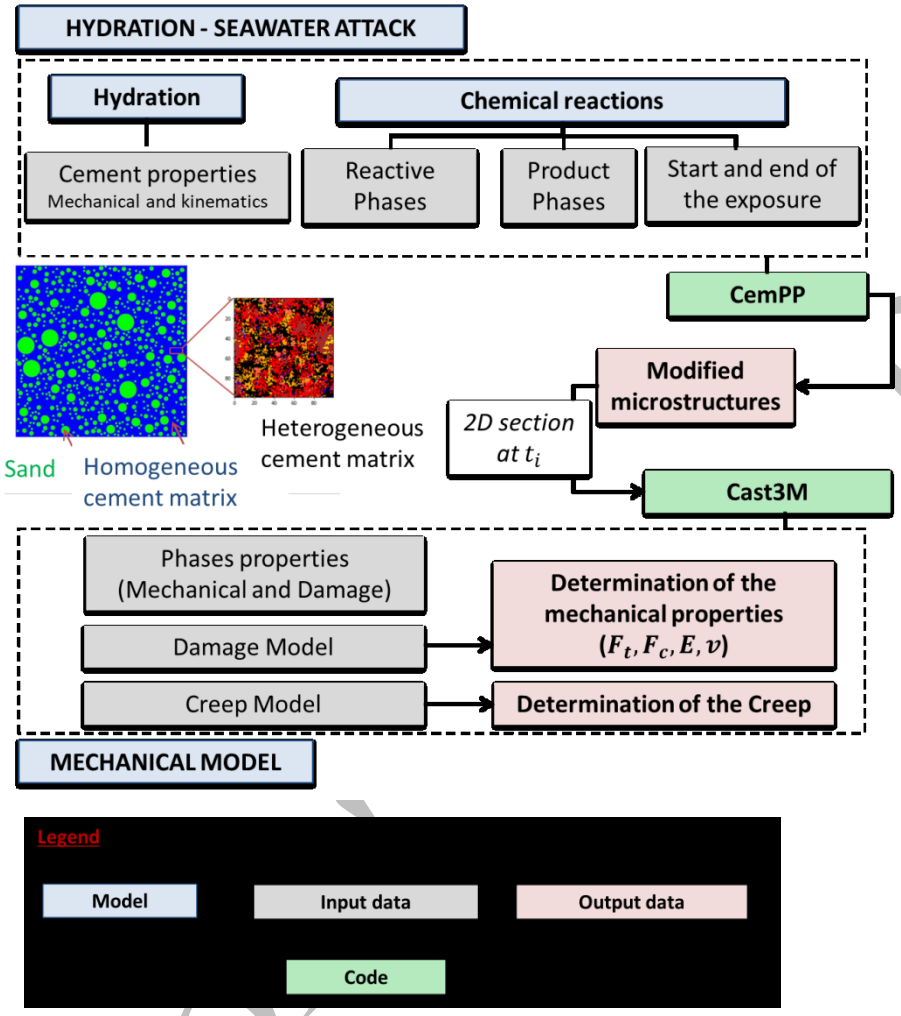

Fig. 1. Algorithm showing the multi-scale chemo mechanical model

After defining the mechanical behaviour of the cement paste, a homogenization method was designed to assess the properties of the mortar. At the mortar scale, the creep-damage model requires the following input parameters: Young's modulus, Poisson's coefficient, strength, rigidity, density, fracture energy and creep coefficients (Elementary rigidity).

The elementary rigidity of the cement paste is determined by a creep simulation as follows. A homogenous cement paste with the same volume size of the heterogeneous volume tested at the lower scale, i.e. 100 µm of length, is created and the same creep test performed on the heterogeneous cement paste is simulated. For the homogenous cement paste the elementary rigidity is required as input data of the model. First of all, an arbitrary value is given and the strain

compliance is compared to that obtained on the heterogeneous volume. Then, the elementary rigidity (creep coefficients) is calibrated to obtain the same compliance curve obtained at the heterogeneous level. This value is finally used at the mortar scale for the cement paste. The representative elementary volume (REV) size of mortar is chosen equal to 5 times the diameter of the biggest inclusion. For the sand used (0-2 mm), the 10mm REV size is adopted.

2.2. Stoichiometric equations of hydration and seawater attack

The cement hydration considers the four basic constituents (C_3S, C_2S, C_3A, C_4AF) of clinker and calcium sulfate, leading to the formation of hydrates as follows (equations 1-8):

$$C_3S + 5.3\,H \rightarrow C_{1.7}SH_4 + 1.3\,CH \quad (1)$$

$$C_2S + 4.3\,H \rightarrow C_{1.7}SH_4 + 0.3\,CH \quad (2)$$

$$C_3A + 6\,H \rightarrow C_3(A,F)SH_6 \quad (3)$$

$$C_4AF + 10\,H \rightarrow C_3(A,F)SH_6 + FH_3 + CH \quad (4)$$

$$C_3A + 3C\bar{S}H_2 + 26\,H \rightarrow C_6A\bar{S}H_{32} \quad (5)$$

$$C_4AF + 3C\bar{S}H_2 + 30\,H \rightarrow C_6A\bar{S}H_{32} + FH_3 + CH \quad (6)$$

$$2C_3A + C_6A\bar{S}H_{32} + 4\,H \rightarrow 3C_4A\bar{S}H_{12} \quad (7)$$

$$2C_4AF + C_6A\bar{S}H_{32} + 12\,H \rightarrow 3C_4A\bar{S}H_{12} + 2FH_3 + 2CH \quad (8)$$

Seawater chemical actions should be described as reactions taking place simultaneously [31], and seawater is composed of several ions forming different products. An experimental study carried out by [14] on ordinary concrete exposed for 10 years in a tidal zone of the Trondheim fjord, shows that the attack progressed in several zones as illustrated in Fig. 2.

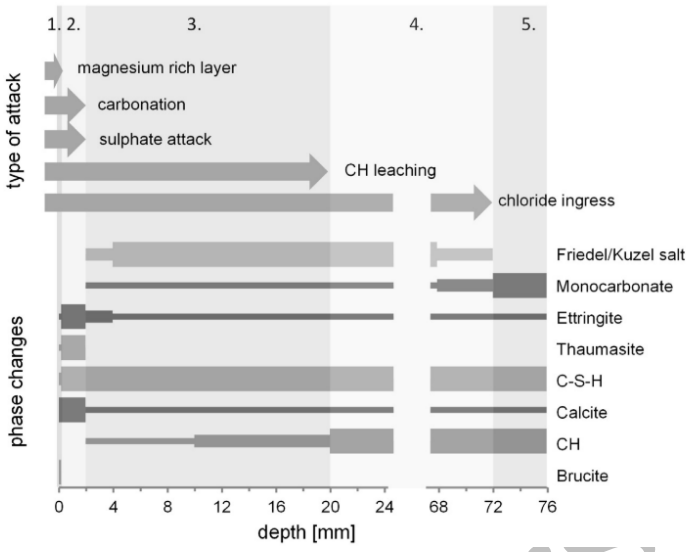

Fig. 2. A schematic overview of the zoned attack caused by seawater in the concrete core and the associated phase changes as a function of depth. (1) Mg enrichment; (2) sulfate attack with ettringite and thaumasite formation and carbonation; (2 and 3) calcium hydroxide leaching; (2–4) chloride ingress; and (5) unaffected concrete extracted from [14]**.**

Seawater contains sulfate and chloride ions. Cement-based materials have higher compressive strength and lower expansion when chloride ions are present in the sulfate solution [13], and their presence can reduce expansion and degradation [17]. It is also known that a higher SO_4^{2-} concentration causes a higher expansion and degradation [12].

A comparison was carried out on the behaviour of concrete subjected to sulfate attack in seawater and in groundwater. It was concluded that mortar has better performance in seawater than in groundwater [17] due to the presence of chloride ions in the first one. Therefore, seawater attack is significantly different from sulfate attack at equivalent sulfate concentrations.

This can be explained by the faster diffusion of chloride ions and their chemical interactions with cement hydration products. The chloride action can lead to the formation of Friedel's and Kuzel's salts via equations 9 and 10 simultaneously:

$$C_3A + Ca(OH)_2 + 2Cl^- + 10H_2O \rightarrow C_3A.CaCl_2.10H_2O + 2\,OH^- \quad (9)$$

Friedel

$$C_3A + 0.5Ca(OH)_2 + 0.5CaSO_4 + 2Cl^- + 10H_2O \rightarrow C_3A.(CaCl_2)_{0.5}.(CaSO_4)_{0.5} \quad (10)$$

Kuzel

The presence of sulfate can lead to the formation of gypsum and ettringite via the following equations 11 and 12:

$$MgSO_4 + Ca(OH)_2 \rightarrow CaSO_4 + Mg(OH)_2 \quad (11)$$

$$CaSO_4 + C_3A + 32H_2O \rightarrow C_3A.3CaSO_4.32H_2O \quad (12)$$

Calcium carbonate $CaCO_3$, precipitates on the surface of concrete in the form of aragonite, vaterite and calcite via the reaction of calcium hydroxide and C-S-H with CO_2 dissolved in seawater as follows (equation 13):

$$Ca(OH)_2 + CO_2 + H_2O \rightarrow Ca\,CO_3 + 2H_2O \quad (13)$$

Seawater also contains Mg^{2+} leading to the formation of a brucite layer on the surface via the following reaction (equation 14):

$$Mg^{2+} + Ca(OH)_2 \rightarrow Mg\,(OH)_2 + Ca^{2+} \quad (14)$$

The formation of brucite and $Ca\,CO_3$ layers can act as protective layers that seal the concrete surface and limit the ionic diffusion into the cement paste.

It is known that thaumasite is formed at low temperatures [14]. Several studies can be found in the literature [32,33]. Research has shown that a low temperature is not necessary for the formation of thaumasite as it be can formed in hot climate regions [34] or at room temperature (25 °C) [35]. The formation of thaumasite directly involves a C-S-H gel, with a source of sulfate and a source of carbonate [35]. Its formation respects the following reaction (equation 15):

$$3CaO.2SiO_2.3\,H_2O + 2(CaSO_4.2H_2O) + CaCO_3 + CO_2 + 23\,H_2O \rightarrow 2\,Ca_3[\,Si(OH)_6\,](CO_3)(SO_4)\,.12\,H_2O \quad (15)$$

2.3. Generation of the attacked microstructure

First of all, using the chemical reactions defined in CEMHYD3D, the simulation of hydration is performed by cycles of dissolution, diffusion, and precipitation.

Secondly, since the chemical action of seawater must be described as one of many reactions taking place simultaneously [31], and since the chemical reaction time has been assumed to be very fast and the characteristic size of the microstructure being very small, a total replacement of the cement

phases by their reaction product is adopted as presented in Table 1. Each layer represents ionic / chemical attack and product formation.

Table 1: Phases replacement considered to model the modified microstructure in the chemical model

	Phases	I	II	III	IV	V	VI	Hydrated
Reactants	Calcium hydroxide							
	CSH							
	Hydrated C_3A							
Products	Brucite							
	Calcite							
	Thaumasite							
	Gypsum							
	Ettringite							
	Friedel Salt							

To understand fully the effect of each phase formed or transformed on the mechanical behaviour of the structure, each layer is simulated separately as a material under hydration-chemical reaction coupling. Then, the multilayer modified microstructure is compared to the hydrated intact one.

The simulation of the hydration-seawater attack coupling process was carried out on $100\mu m^3$ cement paste using CemPP. Similarly to the experimental campaign carried out in [4], the immersion in seawater started at the age of 3 days and the end of exposure is assumed to be 6 months. An Ordinary Portland cement CEMI 52.5 N was simulated. After 6 months the degree of hydration of Portland cement reaches 95% [36], thus the interactions between hydration and seawater attack become less significant.

The mineralogical composition of the cement used as input parameter in CemPP is presented in Table 2. Cement hydration activation energy is considered 40 KJ/mol [37]. Fig. 3 presents an algorithm of the hydration-seawater attack model.

Table 2: Cement mineralogical composition

Cement composition	
	CEMI 52.5 N
C_3S	60.0%
C_2S	16.3%
C_3A	7.7%
C_4AF	10.5%
Gypsum	3.5%
Other contituents	2.0%
Cement properties	
Density (10^3 kg/m^3)	3.16
Blaine fineness (m^2/kg)	400

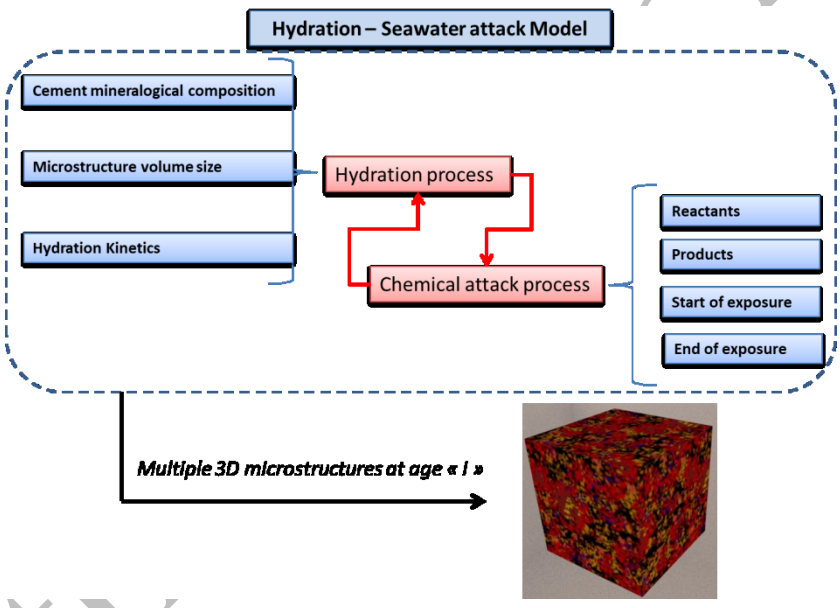

Fig. 3. Algorithm showing the model coupling between hydration and seawater attack

2.4. Definition of the non-linear creep-damage problem

The damage model developed by Fichant et al. [38,39] is adopted to model the damage in the microstructure of cement paste. The input parameters of the micromechanical damage model for each cement paste phase (Young's modulus E, Poisson coefficient v, tensile strength F_t and

fracture energy G_f) were gathered, from the literature, by Rhardane et al. (2020) and they are considered as intrinsic properties to the model.

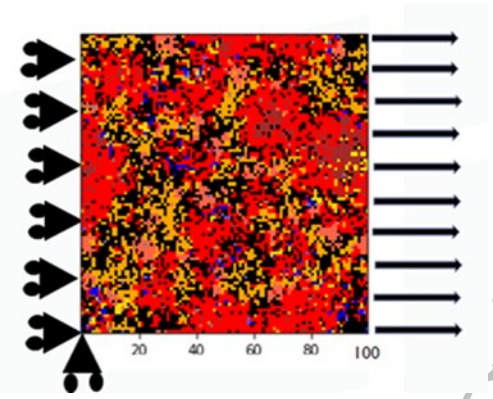

Fig. 4. Boundary conditions applied on a 2D section of cement paste at age ti

The uniaxial load was applied as incremental horizontal displacements on one of the sides of section S while the opposite one is fixed as shown in Fig. 4. The total stress σ is calculated in the isotropic form of the following damage behaviour law (equation 16):

$$\sigma = C^d : \varepsilon^e = (1 - D)\, C^0 : \varepsilon^e \quad (16)$$

where D represents the scalar damage value. It can be defined by the following [39] equation 17:

$$D = 1 - \frac{\kappa_0}{\tilde{\varepsilon}} e^{-B_t(\tilde{\varepsilon} - \kappa_0)} \quad (17)$$

where κ_0 represents the damage threshold and B_t a damage parameter linked to the tensile strength of the material which makes it possible to calculate the softening branch of the stress-strain curve [40]. κ_0 depends on the tensile strength F_t and the Young's modulus E according to the following (equation 18):

$$\kappa_0 = \frac{F_t}{E} \quad (18)$$

B_t depends on the fracture energy G_f according to the energy regularization [41] presented in equation 19:

$$B_t = \frac{hF_t}{G_f} \quad (19)$$

where h represents the element size.

The model equations presented in this section were used to describe each phase present in the cement matrix. The phases properties considered were summarized in [37] and are presented in the **appendix A**.

By applying a constant stress on the structure, creep is modeled using 4 chains of Kelvin Voigt. In the isotropic case, the creep compliance can thus be defined by the following equation 20:

$$J(t) = \sum_{i=1}^{n} \frac{1}{\kappa_i}\left(1 - e^{-\frac{\kappa_i}{\eta_i}t}\right) \quad (20)$$

where $\tau_i = \eta_i/\kappa_i$ represents the characteristics times of the Kelvin-Voigt chains : $\tau_1 = 0{,}1\ day$, $\tau_2 = 1\ day$, $\tau_3 = 10\ days$ et $\tau_4 = 100\ days$.

The only unknown in this relation is the elementary rigidity of each phase k_i. A strong assumption is made here: all phases other than the C-S-H have a negligible viscoelastic behaviour compared to that of the C-S-H. They are then considered as elastic and restrain the deformation of C-S-H. This hypothesis is based on the solidification theory established by [28] for mature cementitious materials. The phases elementary rigidities are summarized in **appendix A** [37].

3. Results analysis

3. 1. Choice of the Representative Elementary Volume

In micromechanical studies it is recommended to use a representative elementary volume size (REV) equal to more than four times the biggest inclusion diameter [42]. In the case of an explicit representation of a cement paste microstructure this condition is difficult to fulfill because there are not inclusions in the definition sense of micromechanics. The REV should be representative for each component . This is possible when these volume fractions are known. In the present study, the cement hydration can be checked only by comparing the hydration degree with experiments but the local volume fractions cannot be compared. That is why the last choice method of the REV cannot be used.

To check the representability of the volume considered, multiple REV sizes (40µm, 80 µm, 100µm and 200µm) have been tested and the phases formed in 3D volume were compared to the average of the phases formed in multiple 2D sections (a section was made each 10 µm in depth). Fig. 5

shows a comparison between 3D and 2D fraction volume calculations for CSH, CH, C_3A and porosity for a REV of 100 μm^3. Results prove that 100 μm^3 is a good compromise between the representability and the calculation time.

It should be noted that 100 μm^3 was used in multiple studies as a default value for hydration models and as a characteristic size for cement pastes in mechanical simulations [43–45].

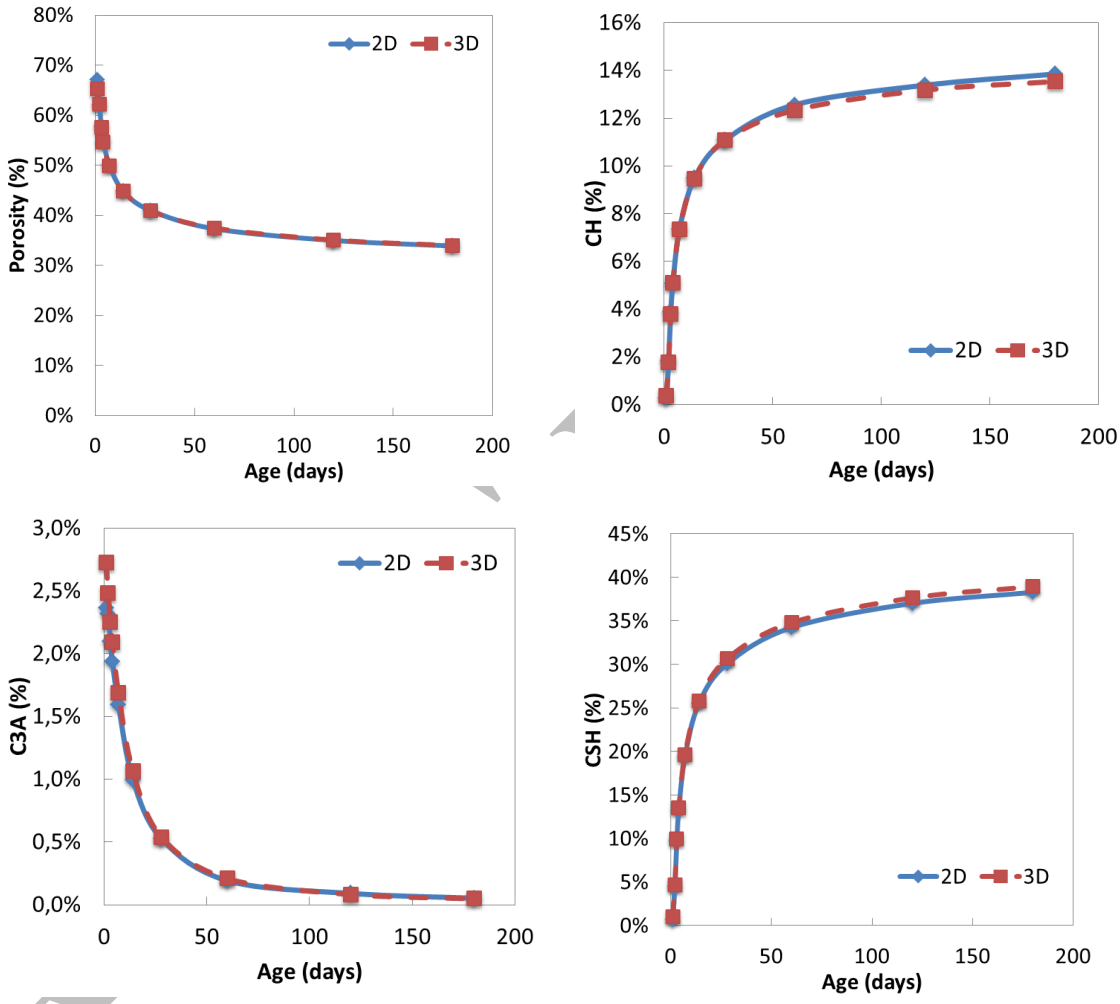

Fig. 5. Volume fraction comparison (in 2D and 3D) of the main phases: a. Porosity, b. CH , c. C_3A and d. CSH

3. 2. Phases changes and their effect on the mechanical behaviour of cement paste

Fig. 6 represents an example of output result obtained from the chemical model at the age of 28 days (a 2D section of the various 3D microstructures generated from CemPP is illustrated in Fig. 6).

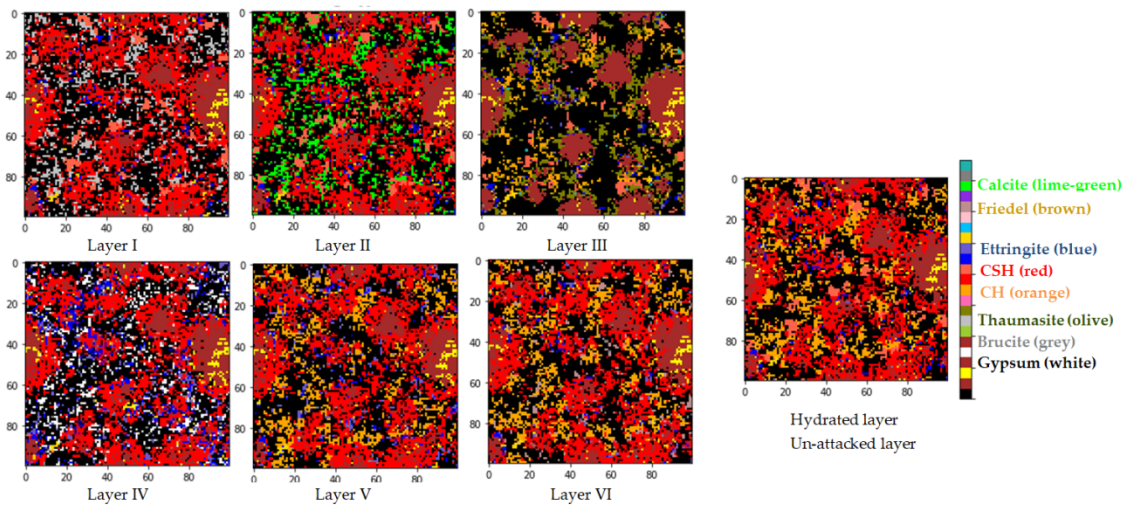

Fig. 6. Output results from the chemical model: 2D sections of each layer extracted from the 3D microstructures generated from CemPP at the age of 28 days.

The color variation between the modified layers and the hydrated un-attacked layer highlights the phase changes in the microstructure:

- Layer I : Brucite-rich layer (Grey color)
- Layer II: Calcite-rich layer (Lime-green color)
- Layer III: Thaumasite-rich layer (Olive color)
- Layer IV: Gypsum-rich layer (White color)
- Layer V: Ettringite-rich layer (Blue color)
- Layer VI: Friedel salt rich layer (Brown color)

Fig. 7 shows the influence of the combined hydration and seawater attack process on the porosity of each layer. Whatever the products formed, the porosity of cement paste decreased due to the formation of hydration products and corresponding volumes of chemically bound water. The highest porosity correspond to layer III, where all C-S-H is assumed to be converted into thaumasite.

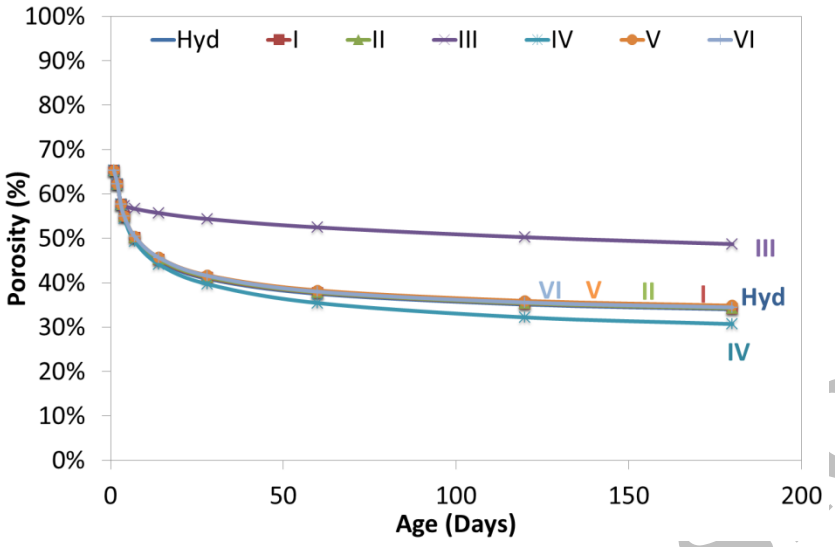

Fig. 7. Evolution of the porosity of cement paste layers as a function of hydration time

Fig. 8 presents the elastic properties variation for the six chemically modified layers and for the hydrated un-attacked layer [46]. It shows a reduction in Poissons's coefficient in all layers except for layer III indicating that the combined hydration and chemical attack result in the decrease of the Poisson's coefficient.

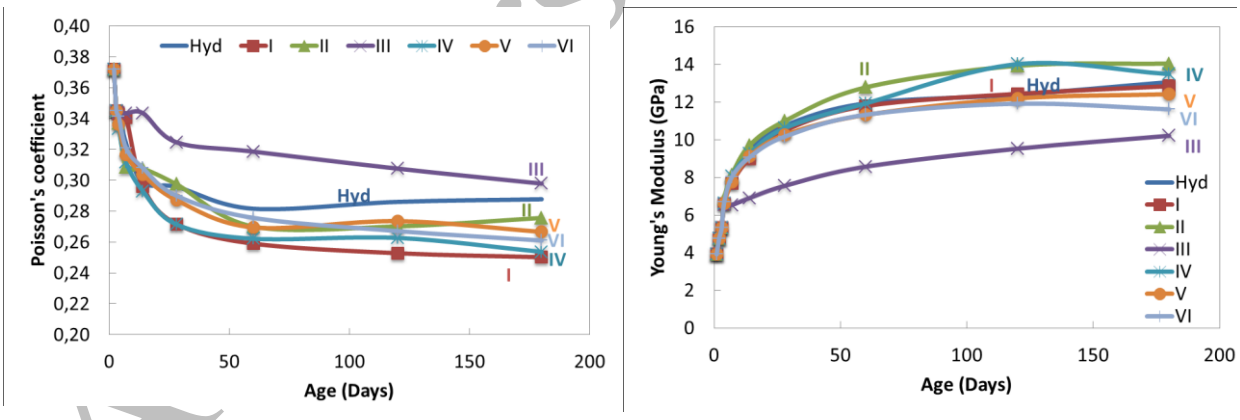

Fig. 8. Elastic parameters variation with time: a. Poisson's coefficient and b. Young's modulus [46]

In Fig. 9 the Young's modulus is plotted against the porosity of each layer at each time indicated in Fig. 7. The graph shows the influence of the phase assemblage of the cement paste on the relationship between porosity and elastic modulus. Young's modulus decreases because of cement hydration but each layer has a different behaviour depending on the phases formed during seawater attacks. This confirms the relevance of modelling strategy taking into account the different fronts

and chemical effects induced by external seawater attack. Fig. 10 represents the compressive (Fig. 10.a) and tensile (Fig. 10.b) strength variations as a function of the microstructures age. The results confirm the influence of microstructural changes on the mechanical behaviour of cement paste layers.

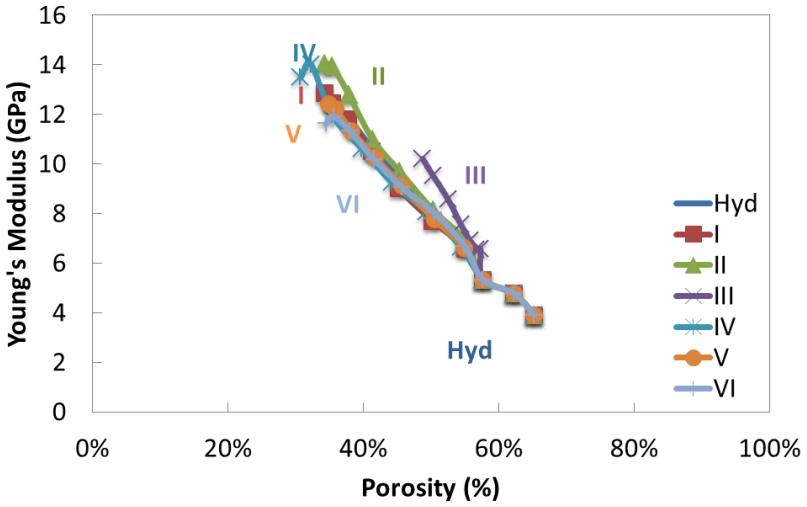

Fig. 9. Correlations between Young's modulus and porosity of cement paste layers.

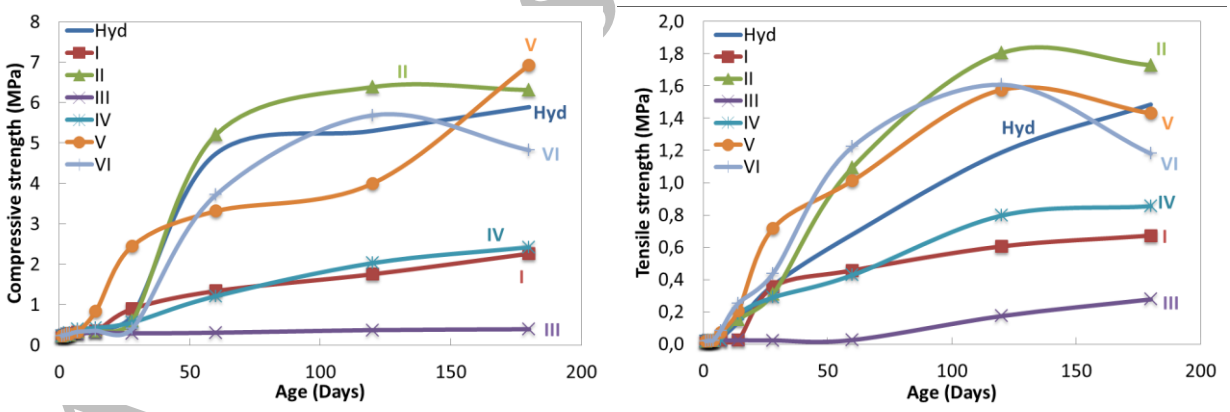

Fig. 10. Layers strength variation with time: a. Compression and b. Traction

It can be seen from Fig. 8 and Fig. 10 that the layer I rich in brucite, acting as a protective layer, maintains a rigidity similar to that of the intact hydrated layer but its compressive and tensile strength decreases.

In layer II, $CaCO_3$ clogs the porosity at the surface and reduces ionic exchanges with the external environment. Higher rigidity and strength are observed in this layer. These results highlight the positive mechanical effects of this protective layer formed.

Layer III is the layer modelling the CSH consumption and thaumasite formation. This layer records the smallest Young's modulus and the largest Poisson's ratio leading to a compressive and tensile strength almost null. In fact, this is due to the consumption of the main hydration product, therefore preventing the strength and rigidity improvements of the microstructure with time.

The action of sulfate ions leading to the formation of gypsum (layer IV) increases the rigidity of the layer but reduces its strength.

The reaction of the hydrated C_3A with the ions present in seawater disrupts the behaviour law of the two layers V (rich in ettringite) and VI (rich in Friedel's salt), but these layers maintain a Young's modulus similar to that of the un-attacked one. Young's modulus evolutions curves remained almost similar in all layers: an increase is recorded in the first days than the modulus remained almost constant. A decrease in Young's modulus after 6 months of exposure was recorded. The compressive strength evolution for layers V (rich in ettringite) and VI (rich in Friedel's salt) did not stabilize like the other layers, but it increased at the age of 2 months then decreased at the age of 6 months highlighting the importance of the reaction with the hydrated C_3A.

3. 3. Effect of phases assemblage on the mechanical behaviour of cement paste

Comparing the cement paste structure attacked by seawater to an intact one was achieved using a multilayer cement volume of 100 μm^3, where each layer chemically modified is modelled as 10 µm in depth. The layers thickness variations as a function of time have not been taken into account in this section. Therefore, two microstructures of cement pastes were modelled:

- An intact hydrated cement paste microstructure
- A multi-layered microstructure assembling the seven layers studied in section III.2

Fig. 11 and Fig. 12 show the variation in elastic properties (Poisson's ratio in Fig. 11.a and Young's modulus in Fig. 11.b) and strength (Compressive in Fig. 12.a and tensile in Fig. 12.b) of the modelled intact and chemically modified microstructures, respectively.

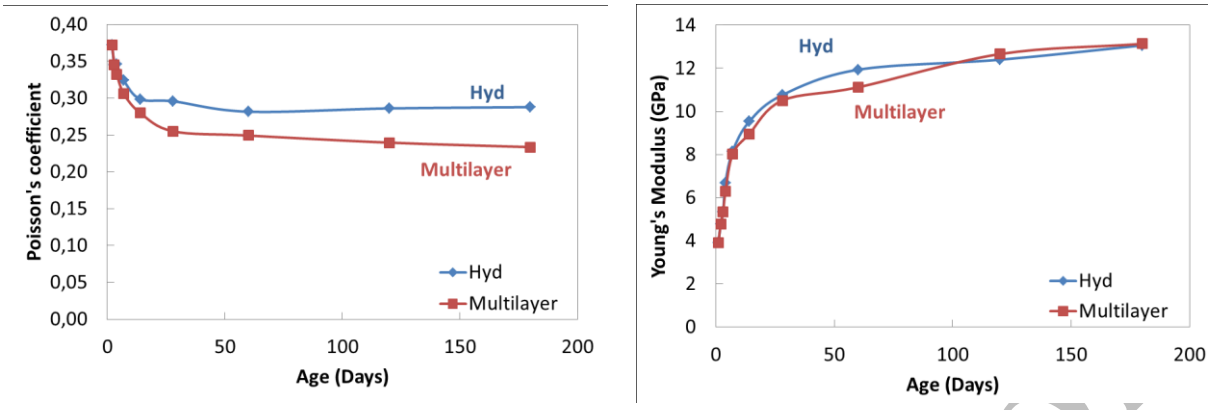

Fig. 11. Elastic parameters variation with time for the hydrated and modified microstructure: a. Poisson's coefficient and b. Young's modulus

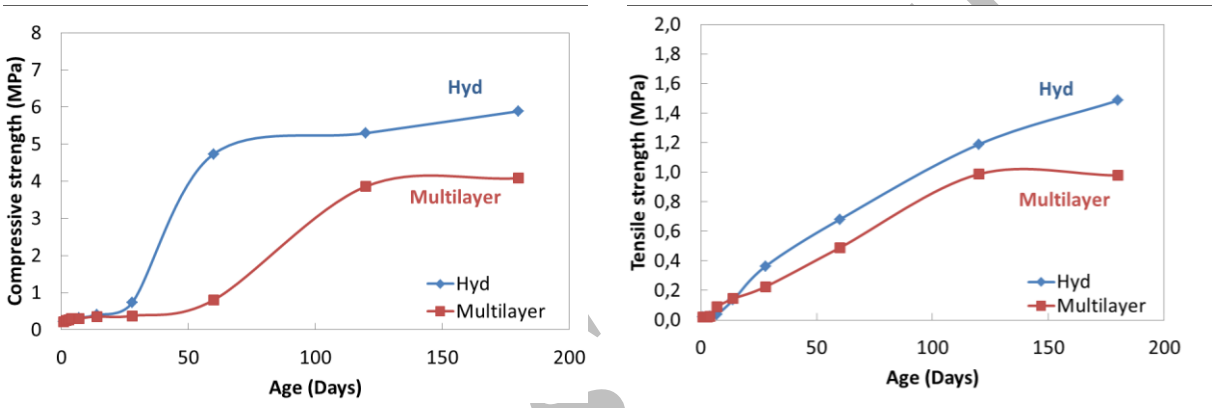

Fig. 12. Strength variation with time for the hydrated and modified microstructure: a. Compression and b. Tension

Similarly to the results obtained in Fig. 11.a, the seawater attack reduces the global Poisson's ratio of the exposed microstructure (Fig. 11.a). As for the Young's modulus, it remains the same in both microstructures (Fig. 11.b).

It can be seen from Fig. 12 that the seawater attack reduces the global strength of the cement paste. However, at the microscopic level of the attacked layers a competition took place between strength and rigidity of each layer (Fig. 8 and Fig. 10). Some layers recorded a higher strength and others a lower strength.

3. 4. Creep analysis of the attacked cement paste

Fig. 13 shows the C-S-H percentages in each layer at the loading age (28 days) and the creep compliance variation for 3 years of loading. The load applied is equivalent to 30% of the structure strength at the age of loading.

It can be seen that the creep compliance increases rapidly during the first days of loading and then it follows an asymptotic evolution, describing a low viscoelastic displacement.

The brucite-rich layer modeled in layer I and the $CaCO_3$-rich layer modeled in layer II record a lower creep compliance than the intact hydrated microstructure.

The layer III records a negligible creep compliance. This can be explained by the fact that the viscoelastic behaviour of C-S-H was considered while the other components remained elastic. Therefore, the absence of C-S-H in this layer implies a negligible creep. It is noteworthy to mention that this layer is also characterized by higher porosity (Fig. 7) and lower Young's modulus, thus potentially higher elastic deformation.

The layer IV, modelling the gypsum formation, records the smallest amount of C-S-H (29.47%), after the layer III, and therefore the second smallest creep compliance (with a maximal value of 656 μm/m/MPa).

The layer V, modelling the ettringite rich layer, records a creep compliance similar to the un-attacked layer.

The layer VI, modelling the chlorides action and the Friedel's salt formation, has a creep compliance similar to layers I and II and lower than the un-attacked layer. The maximum creep compliance recorded after 3 years of loading reaches 650-850 μm/m/MPa).

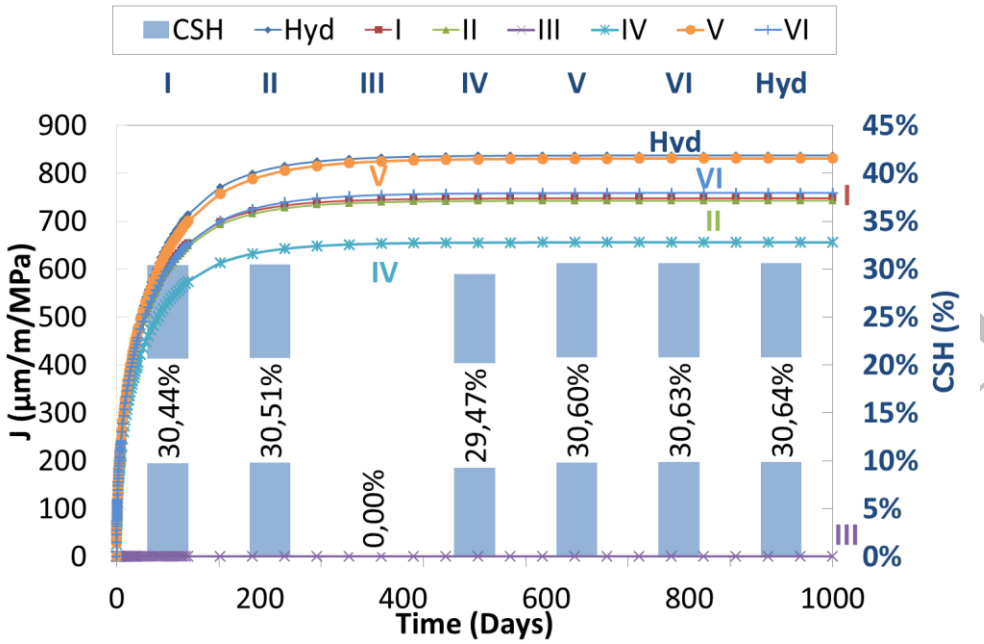

Fig. 13. Creep compliance and CSH percentages of all the layers loaded at the age of 28 days

In addition, simulations of creep were performed for cement pastes loaded at 4 and 6 months (Fig. 14). It can be seen that there is no difference in the creep compliance between these two loading ages. It is because the microstructure has gained its strength and rigidity and C-S-H percentage does not increase significantly between these two loading ages.

It can also be concluded from these figures that the ettringite rich layer recorded the highest creep and that the gypsum rich layer recorded the lowest creep at all ages of load application due the lowest amount of C-S-H.

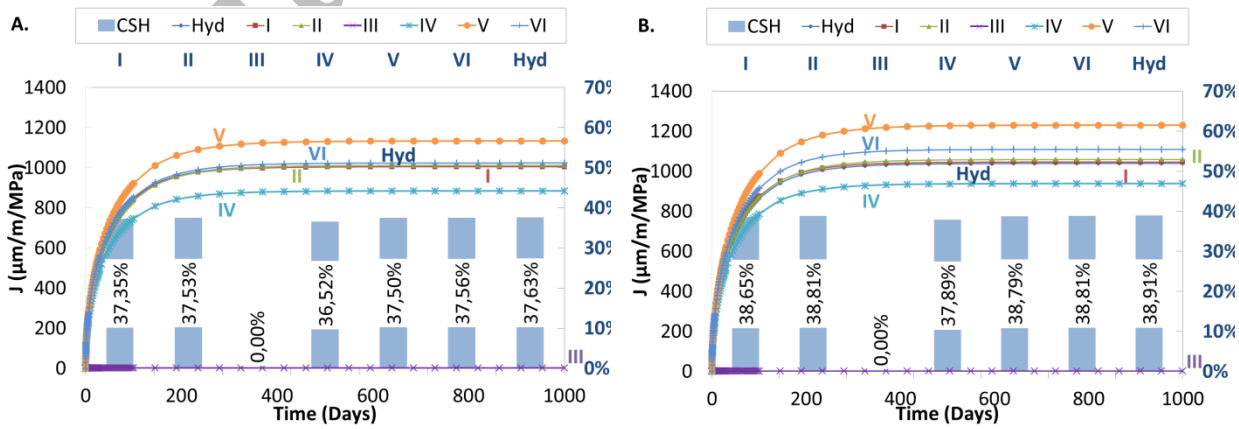

Fig. 14. Creep compliance and CSH percentages of all the layers loaded at the age of (A) 4 months and (B) 6 months

3. 5. Results analysis of attacked mortars

Using the results obtained at the scale of cement paste, a homogeneous matrix was modeled using one phase.

The creep coefficient "K_i" values were determined by performing multiple simulations (trial and error). The "K_i'' adopted for mortar simulations are the ones that give the creep curve that fits the best with the heterogeneous cement matrix compliance curve.

As for the compressive and tensile strength, Young's modulus and Poisson's coefficient, the values obtained using the heterogeneous material were adopted.

The sand elastic properties (Young's modulus and Poisson's coefficient) have been obtained from an inverse analysis of elastic test on a mortar sample: E_s = 78 GPa, ν_s = 0.2 [20]. Sand particles have diameters between 0 and 2mm, a density of 2.61 g/cm^3 and represent 30% of the specimen volume.

Fig. 15 and Fig. 16 show a comparison of the strength and rigidity of mortar and cement paste at the age of 28 days.

The results highlight the effect of aggregates in the mechanical performance improvement of the structures [47–49]. From the compressive strength results, mortar actually shows a higher strength than cement paste for both hydrated and multilayer specimens (Fig. 16). Similarly, a higher Young's modulus was recorded in the case of mortar volumes (Fig. 15).

These figures also show that the strength of the chemically modified mortar is significantly lower than the intact hydrated mortar. This is due to the formation of phases that have a lower strength (in particularly layers I, III and IV presented in Fig. 10). It is also noteworthy to mention that simulations were performed with a percentage of phase's modification of 100%, representing a high level of seawater degradation and therefore they could represent long-term immersion. The thickness of all the layers were taken equal, which also results in a high overall degree of degradation.

As for rigidity, similar values were recorded between modified and intact volumes. This can be explained at the microstructure level (Fig. 8) where the chemically modified layers have almost a similar elastic modulus.

These results clearly highlight that the phenomena affecting the strength and rigidity of cement-based materials are different. The evolution of Young's modulus is mainly affected by the evolution of porosity (Fig. 7) and the modulus of the different phases. The evolution of strength is more complex, however it should be taken into account to describe accurately the mechanical behaviour of seawater attacked concrete structures.

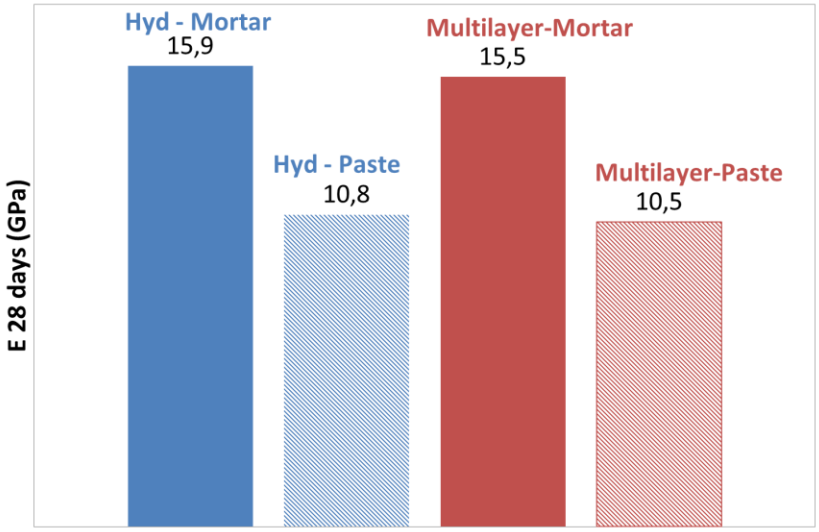

Fig. 15. Comparison between mortar and cement paste rigidity calculated at the age of 28 days

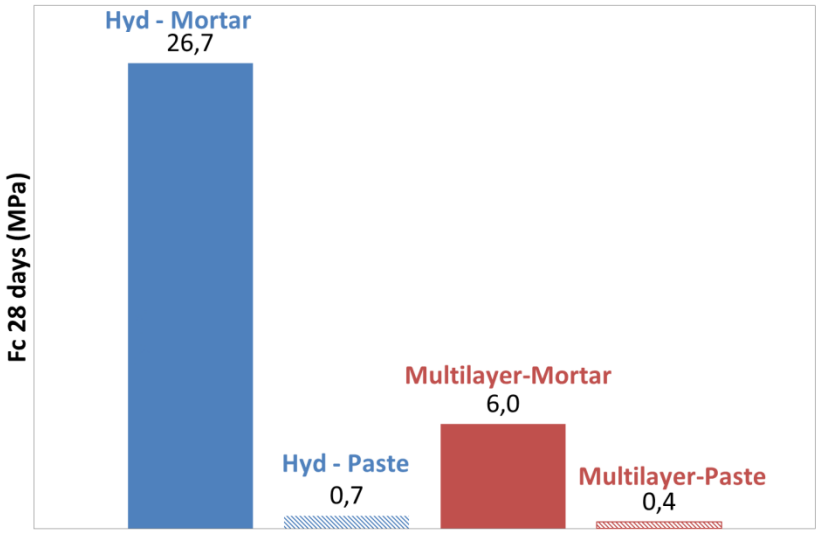

Fig. 16. Comparison between mortar and cement paste compressive strength calculated at the age of 28 days

4. Conclusions

The aim of this study was to provide a tool for the rapid mechanical evaluation of offshore structures and therefore a tool that can be used for the optimization and the development of durable marine constructions. Therefore microscopic and mesoscopic behaviour laws have been presented and studied for cement-based material exposed to seawater and mechanical loading.

Results show the rigidity and strength evolution at the microscopic level. These parameters lead to a global mechanical evaluation at the mortar level, where a significant decrease in strength was recorded for structures immerged in seawater. The microscopic evaluation helps understanding the effect of each ion on the mechanical evaluation of the structure. It also highlights the competition between protective and damaged layers observed in marine environment [5,14]. Therefore, results show that the overall behaviour of a structure is influenced by the chemically modified phases and, it is therefore possible to outline the maximum permissible load as a function of the chemical degradation level of the structure.

In addition, creep tests were performed at the microscopic level after different exposure periods by adapting the load at each time. In accordance with the creep results, we can conclude that the amount of C-S-H formed or transformed is linked to the creep deformations recorded. This can be explained by the model creep assumptions for which C-S-H has a high viscoelastic behaviour in comparison with the other components considered elastic.

This modelling method highlights the importance of examining all ions in seawater since each ion participates in either a gain or a loss in elastic properties, affecting the behaviour of the structure.

While this model seems promising and presents information on the chemo-mechanical evaluation of offshore structures, coupling between chemical and mechanical evaluation is a challenge that is worth further evaluations. Additional applications for the model could be established to understand better the creep mechanism for offshore structures.

References

[1] Zhang X, Zuo G, Memon SA, Xing F, Sun H. Effects of initial defects within mortar cover on corrosion of steel and cracking of cover using X-ray computed tomography. Construction and Building Materials 2019;223:265–77. https://doi.org/10.1016/j.conbuildmat.2019.06.172.

[2] Sun H, Jiang C, Cao K, Yu D, Liu W, Zhang X, et al. Monitoring of steel corrosion and cracking in cement paste exposed to combined sulfate–chloride attack with X-ray microtomography. Construction and Building Materials 2021;302:124345. https://doi.org/10.1016/j.conbuildmat.2021.124345.

[3] Tian Y, Wen C, Wang G, Hu J, Mai Z. Marine field test for steel reinforcement embedded in mortar: Coupled influence of the environmental conditions on corrosion. Marine Structures 2020;73:102788. https://doi.org/10.1016/j.marstruc.2020.102788.

[4] El-Khoury M, Roziere E, Grondin F, Cortas R, Hage Chehade F. Experimental evaluation of the effect of cement type and seawater salinity on concrete offshore structures. Construction and Building Materials 2022;322:126471. https://doi.org/10.1016/j.conbuildmat.2022.126471.

[5] Guillon E. Durabilité des matériaux cimentaires: modélisation de l'influence des équilibres physico-chimiques sur la microstructure et les propriétés mécaniques résiduelles. École Normale Supérieure de Cachan, 2004.

[6] Massaad G, Rozière E, Loukili A, Izoret L. Advanced testing and performance specifications for the cementitious materials under external sulfate attacks. Construction and Building Materials 2016;127:918–31.

https://doi.org/10.1016/j.conbuildmat.2016.09.133.

[7] Cefis N, Comi C. Damage modelling in concrete subject to sulfate attack. Frattura Ed Integrita Strutturale 2014;8:222–9. https://doi.org/10.3221/IGF-ESIS.29.19.

[8] Rozière E, Loukili A, El Hachem R, Grondin F. Durability of concrete exposed to leaching and external sulphate attacks. Cement and Concrete Research 2009;39:1188–98. https://doi.org/10.1016/j.cemconres.2009.07.021.

[9] Idiart AE, Carol I, López CM, Murcia J. Computational modeling of external sulfate attack in concrete at the meso-level. In: (Eds) EO and DRJO, editor. X International Conference on Computational Plasticity, Barcelona,: 2009, p. 0–4. https://doi.org/10.1111/j.1744-7909.2010.01020.x.

[10] Collepardi M. A state-of-the-art review on delayed ettringite attack on concrete. Cement and Concrete Composites 2003;25:401–7. https://doi.org/10.1016/S0958-9465(02)00080-X.

[11] Harrison WH. Effect of chloride in mix ingredients on sulphate resistance of concrete. Magazine of Concrete Research 1990;42:113–26. https://doi.org/10.1680/macr.1990.42.152.113.

[12] Zhang M, Chen J, Lv Y, Wang D, Ye J. Study on the expansion of concrete under attack of sulfate and sulfate – chloride ions. Construction and Building Materials 2013;39:26–32. https://doi.org/10.1016/j.conbuildmat.2012.05.003.

[13] Al-Amoudi OSB, Maslehuddin M, Abdul-al Y. AB. Role of chloride ions on expansion and strength reduction in plain and blended cements in sulfate environments. Construction and Building Materials 1995;9:25–33.

[14] De Weerdt K, Justnes H, Geiker MR. Changes in the phase assemblage of concrete exposed to sea water. Cement and Concrete Composites 2014;47:53–63. https://doi.org/10.1016/j.cemconcomp.2013.09.015.

[15] Brown PW, Doerr A. Chemical changes in concrete due to the ingress of aggressive species. Cement and Concrete Research 2000;30:411–8. https://doi.org/10.1016/S0008-8846(99)00266-5.

[16] Hartwich P, Vollpracht A. Influence of leachate composition on the leaching behaviour of concrete. Cement and Concrete Research 2017;100:423–34. https://doi.org/10.1016/j.cemconres.2017.07.002.

[17] Santhanam M, Cohen M, Olek J. Differentiating seawater and groundwater sulfate attack in Portland cement mortars. Cement and Concrete Research 2006;36:2132–7. https://doi.org/10.1016/j.cemconres.2006.09.011.

[18] Touil B, Ghomari F, Khelidj A, Bonnet S, Amiri O. Durability assessment of the oldest concrete structure in the Mediterranean coastline: The Ghazaouet harbour. Marine Structures 2022;81:1–19. https://doi.org/10.1016/j.marstruc.2021.103121.

[19] Rhardane A, Grondin F, Alam SY. Numerical simulation of microcracking induced by drying shrinkage in early age cement pastes. 10th International Conference on Fracture Mechanics of Concrete and Concrete Structures, 2019. https://doi.org/10.21012/fc10.235657.

A. Rhardane, S.-Y. Alam, F. Grondin, 'The role of surface micro-cracks in cementitious materials responsible for the Pickett effect', Mechanics of Time Dependent Materials (Q2), 2021, https://doi.org/10.1007/s11043-021-09509-w.

[20] Rhardane A, Alam SY, Grondin F. Microscopically informed upscale approach of modelling damage in mortar by considering matrix-to-grain interface and grain micro-fracture characteristics. Theoretical and Applied Fracture Mechanics 2020;109:102725. https://doi.org/10.1016/j.tafmec.2020.102725.

[21] Rhardane A, Grondin F, Alam SY. Development of a micro-mechanical model for the determination of damage properties of cement pastes. Construction and Building Materials 2020;261:120514. https://doi.org/10.1016/j.conbuildmat.2020.120514.

[22] Hilloulin B, Hilloulin D, Grondin F, Loukili A, De Belie N. Mechanical regains due to self-healing in cementitious materials: Experimental measurements and micro-mechanical model. Cement and Concrete Research 2016;80:21–32. https://doi.org/10.1016/j.cemconres.2015.11.005.

[23] Verpaux P, Charras T, Millard A. CASTEM 2000 une approche moderne du calcul des

structures. Calcul des structures et intelligences artificielle, 1998.

[24] Rhardane A, Alam SY, Grondin F. The role of surface micro-cracks in cementitious materials responsible for the Pickett effect. Mechanics of Time-Dependent Materials 2021. https://doi.org/10.1007/s11043-021-09509-w.

[25] Guo M, Hu B, Xing F, Zhou X, Sun M, Sui L, et al. Characterization of the mechanical properties of eco-friendly concrete made with untreated sea sand and seawater based on statistical analysis. Construction and Building Materials 2020;234:117339. https://doi.org/10.1016/j.conbuildmat.2019.117339.

[26] Saliba J, Grondin F, Matallah M, Loukili A, Boussa H. Relevance of a mesoscopic modeling for the coupling between creep and damage in concrete. Mechanics of Time-Dependent Materials 2013;17:481–99. https://doi.org/10.1007/s11043-012-9199-4.

[27] Guo M, Grondin F, Loukili A. Numerical method to model the creep of recycled aggregate concrete by considering the old attached mortar. Cement and Concrete Research 2019;118:14–24. https://doi.org/10.1016/j.cemconres.2019.01.008.

[28] Bazant ZP, Prasannan S. Solidification theory for aging creep. I : Formulation. Journal of Engineering Mechanics 1989;115:1691–703.

[29] Saliba J, Matallah M, Loukili A, Grondin F, Boussa H. Modelling of basic creep effect on concrete damage at a mesoscale level. First ECCOMAS Young Investigators Conference, 2012.

[30] Bentz DP. A Three-Dimensional Cement Hydration and Microstructure Program. I. Hydration Rate, Heat of Hydration, and Chemical Shrinkage. NISTIR 5756; 1995.

[31] Eglinton M. Resistance of concrete to destructive agencies. In: Hewlett PC, editor. Lea's Chemistry of Cement and Concrete - Fourth Edition, Elsevier Ltd.; 1998, p. 299–342. https://doi.org/10.1016/B978-0-08-100773-0.00006-X.

[32] Schmidt T, Lothenbach B, Romer M, Neuenschwander J, Scrivener K. Physical and microstructural aspects of sulfate attack on ordinary and limestone blended Portland cements. Cement and Concrete Research 2009;39:1111–21. https://doi.org/10.1016/j.cemconres.2009.08.005.

[33] Schmidt T, Lothenbach B, Romer M, Scrivener K, Rentsch D, Figi R. A thermodynamic and experimental study of the conditions of thaumasite formation. Cement and Concrete Research 2008;38:337–49. https://doi.org/10.1016/j.cemconres.2007.11.003.

[34] Diamond S, Lee RJ. Microstructural alterations associated with sulfate attack in permeable concretes. In: J. S, J. M, editors. In: , Editors, Material Science of Concrete - Sulfate Attack Mechanisms, Westerville,: American Ceramic Society; 1999, p. 123–74.

[35] Santhanam M, Cohen MD, Olek J. Effects of gypsum formation on the performance of cement mortars during external sulfate attack. Cement and Concrete Research 2003;33:325–32.

[36] Cardinaud G, Rozière E, Martinage O, Loukili A, Barnes-Davin L, Paris M, et al. Calcined clay – Limestone cements: Hydration processes with high and low-grade kaolinite clays. Construction and Building Materials 2021;277:122271. https://doi.org/10.1016/j.conbuildmat.2021.122271.

[37] Rhardane A. Élaboration d'une approche micromécanique pour modéliser l'endommagement des matériaux cimentaires sous fluage et cycles de gel-dégel. Ecole Centrale de Nantes, 2018.

[38] Fichant S, La Borderie C, Pijaudier-cabot G. Isotropic and anisotropic descriptions of damage in concrete structures. Mechanics of Cohesive Frictional Materials 1999;4:339–59.

[39] Fichant S, Pijaudier-cabot G, La Borderie C. Continuum damage modelling : Approximation of crack induced anisotropy. Mechanics Research Communications 1997;24:109–14.

[40] Mazars J. Application de la mécanique de l'endommagement au comportement non linéaire et à la rupture du béton de structure. Université Pierre et Marie Curie, 1984.

[41] Matallah M, Farah M, Grondin F, Loukili A, Rozière E. Size-independent fracture energy of concrete at very early ages by inverse analysis. Engineering Fracture Mechanics 2013;109:1–16. https://doi.org/10.1016/j.engfracmech.2013.05.016.

[42] Grondin F, Dumontet H, Hamida A Ben, Mounajed G, Boussa H. Multi-scales modelling for the behaviour of damaged concrete. Cement and Concrete Research 2007;37:1453–62.

https://doi.org/10.1016/j.cemconres.2007.05.012.

[43] Ouyang X, Ye G, van Breugel K. Experimental and numerical evaluation of mechanical properties of interface between filler and hydration products. Construction and Building Materials 2017;135:538–49. https://doi.org/10.1016/j.conbuildmat.2017.01.022.

[44] Zhang H, Šavija B, Figueiredo SC, Lukovic M, Schlangen E. Microscale testing and modelling of cement paste as basis for multi-scale modelling. Materials 2016;9. https://doi.org/10.3390/ma9110907.

[45] Bernard F, Kamali-Bernard S. Performance simulation and quantitative analysis of cement-based materials subjected to leaching. Computational Materials Science 2010;50:218–26. https://doi.org/10.1016/j.commatsci.2010.08.002.

[46] El-Khoury M, Grondin F, Rozière E, Cortas R, Hage Chehade F. Chemo-mechanical coupling model of off-shore concrete structures. Academic Journal of Civil Engineering 2021;39:39–42.

[47] de Larrard F, Sedran T. Optimization of ultra-high-performance concrete by the use of a packing model. Cement and Concrete Research 1994;24:997–1009. https://doi.org/10.1016/0008-8846(94)90022-1.

[48] de Larrard F, Tondat P. Sur la contribution de la topologie du squelette granulaire à la résistance en compression du béton. Materials and Structures 1993;26:505–16. https://doi.org/10.1007/BF02472861.

[49] de Larrard F. Structures granulaires et formulation des bétons. 1999.

Appendix A

Phase ID	*E (Pa)*	*HD (Pa)*	*v*	*MV (Kg/m3)*	*K1 (Pa)*	*K2 (Pa)*	*K3 (Pa)*	*K4 (Pa)*	*ETA1 (Pa)*
POROSITY	1.9000E+09	1.0000E+06	4.9992E-01	9.9707E+02	1.0000E+30	1.0000E+30	1.0000E+30	1.0000E+30	2.4400E+42
C3S	1.3740E+11	8.7000E+09	2.9900E-01	3.1500E+03	1.0000E+30	1.0000E+30	1.0000E+30	1.0000E+30	2.4400E+42
C2S	1.3546E+11	8.0000E+09	2.9700E-01	3.2700E+03	1.0000E+30	1.0000E+30	1.0000E+30	1.0000E+30	2.4400E+42
C3A	1.4523E+11	1.0800E+10	2.7800E-01	3.0380E+03	1.0000E+30	1.0000E+30	1.0000E+30	1.0000E+30	2.4400E+42
C4AF	1.5076E+11	9.5000E+09	3.1800E-01	3.7300E+03	1.0000E+30	1.0000E+30	1.0000E+30	1.0000E+30	2.4400E+42
GYPSUM	4.4530E+10	5.9820E+08	3.3000E-01	2.3200E+03	1.0000E+30	1.0000E+30	1.0000E+30	1.0000E+30	2.4400E+42
HEMIHYD	1.3200E+11	1.2456E+09	2.5000E-01	2.7300E+03	1.0000E+30	1.0000E+30	1.0000E+30	1.0000E+30	2.4400E+42
ANHYDRITE	8.8780E+10	1.8930E+09	2.3300E-01	2.9700E+03	1.0000E+30	1.0000E+30	1.0000E+30	1.0000E+30	2.4400E+42
SFUME	7.2050E+10	7.0000E+09	1.6800E-01	2.2000E+03	1.0000E+30	1.0000E+30	1.0000E+30	1.0000E+30	2.4400E+42
BRUCITE	8.3290E+10	1.0000E+09	1.8300E-01	2.3900E+03	1.0000E+30	1.0000E+30	1.0000E+30	1.0000E+30	2.4400E+42
THAUMASITE	4.5055E+10	3.5000E+09	3.1000E-01	1.6780E+03	1.0000E+30	1.0000E+30	1.0000E+30	1.0000E+30	2.4400E+42
ASG	7.1680E+10	7.0000E+09	1.6900E-01	3.2470E+03	1.0000E+30	1.0000E+30	1.0000E+30	1.0000E+30	2.4400E+42
CaS2	7.1680E+10	7.0000E+09	1.6900E-01	2.7700E+03	1.0000E+30	1.0000E+30	1.0000E+30	1.0000E+30	2.4400E+42
CH	4.3480E+10	1.4935E+09	2.9400E-01	2.2400E+03	1.0000E+30	1.0000E+30	1.0000E+30	1.0000E+30	2.4400E+42
CSH	2.3800E+10	1.1100E+09	2.4000E-01	2.1100E+03	1.2000E+10	7.2000E+09	4.8000E+09	9.5000E+07	2.4400E+21
C3AH6	9.3838E+10	6.5600E+09	3.2000E-01	2.5200E+03	1.0000E+30	1.0000E+30	1.0000E+30	1.0000E+30	2.4400E+42
ETTR	2.4090E+10	7.9910E+08	3.2100E-01	1.7800E+03	1.0000E+30	1.0000E+30	1.0000E+30	1.0000E+30	2.4400E+42
ETTRC4AF	2.4090E+10	7.9910E+08	3.2100E-01	1.7800E+03	1.0000E+30	1.0000E+30	1.0000E+30	1.0000E+30	2.4400E+42
AFM	4.3151E+10	5.3000E+09	2.9173E-01	2.0100E+03	1.0000E+30	1.0000E+30	1.0000E+30	1.0000E+30	2.4400E+42
FH3	2.2400E+10	5.9040E+09	2.5000E-01	3.0620E+03	1.0000E+30	1.0000E+30	1.0000E+30	1.0000E+30	2.4400E+42
POZZCSH	2.3800E+10	1.1100E+09	2.4000E-01	2.1100E+03	1.2000E+10	7.2000E+09	4.8000E+09	9.5000E+07	2.4400E+21

SLAGCSH	2.3800E+10	1.1100E+09	2.4000E-01	2.1100E+03	1.2000E+10	7.2000E+09	4.8000E+09	9.5000E+07	2.4400E+21
CACL2	4.2300E+10	1.4000E+09	3.2400E-01	2.1500E+03	1.0000E+30	1.0000E+30	1.0000E+30	1.0000E+30	2.4400E+42
FRIEDEL	2.2400E+10	1.5400E+09	2.5000E-01	1.8920E+03	1.0000E+30	1.0000E+30	1.0000E+30	1.0000E+30	2.4400E+42
STRAT	2.2400E+10	6.6295E+09	2.5000E-01	1.9400E+03	1.0000E+30	1.0000E+30	1.0000E+30	1.0000E+30	2.4400E+42
GYPSUMS	4.4530E+10	5.9820E+08	3.3000E-01	2.3200E+03	1.0000E+30	1.0000E+30	1.0000E+30	1.0000E+30	2.4400E+42
CACO3	9.6960E+10	1.4000E+09	2.9600E-01	2.7100E+03	1.0000E+30	1.0000E+30	1.0000E+30	1.0000E+30	2.4400E+42
AFMC	7.8950E+10	5.3000E+09	2.5000E-01	2.1400E+03	1.0000E+30	1.0000E+30	1.0000E+30	1.0000E+30	2.4400E+42
INERTAGG	2.3800E+10	1.1100E+09	2.4000E-01	2.1100E+03	1.2000E+10	7.2000E+09	4.8000E+09	9.5000E+07	2.4400E+21
ABSGYP	4.4530E+10	5.9820E+08	3.3000E-01	2.3200E+03	1.0000E+30	1.0000E+30	1.0000E+30	1.0000E+30	2.4400E+42
DIFFCSH	2.3800E+10	1.1100E+09	2.4000E-01	2.1100E+03	1.2000E+10	7.2000E+09	4.8000E+09	9.5000E+07	2.4400E+21
DIFFCH	4.3480E+10	1.4935E+09	2.9400E-01	2.2400E+03	1.0000E+30	1.0000E+30	1.0000E+30	1.0000E+30	2.4400E+42
DIFFGYP	4.4530E+10	5.9820E+08	3.3000E-01	2.3200E+03	1.0000E+30	1.0000E+30	1.0000E+30	1.0000E+30	2.4400E+42
DIFFC3A	1.4523E+11	1.0800E+10	2.7800E-01	3.0380E+03	1.0000E+30	1.0000E+30	1.0000E+30	1.0000E+30	2.4400E+42
DIFFC4A	1.5076E+11	9.5000E+09	3.1800E-01	3.7300E+03	1.0000E+30	1.0000E+30	1.0000E+30	1.0000E+30	2.4400E+42
DIFFFH3	2.2400E+10	5.9040E+09	2.5000E-01	3.0620E+03	1.0000E+30	1.0000E+30	1.0000E+30	1.0000E+30	2.4400E+42
DIFFETTR	2.4090E+10	7.9910E+08	3.2100E-01	1.7800E+03	1.0000E+30	1.0000E+30	1.0000E+30	1.0000E+30	2.4400E+42
DIFFCACO3	9.6960E+10	1.4000E+09	2.9600E-01	2.7100E+03	1.0000E+30	1.0000E+30	1.0000E+30	1.0000E+30	2.4400E+42
DIFFAS	2.3800E+10	1.1100E+09	2.4000E-01	2.1100E+03	1.2000E+10	7.2000E+09	4.8000E+09	9.5000E+07	2.4400E+21
DIFFANH	2.3800E+10	1.1100E+09	2.4000E-01	2.1100E+03	1.2000E+10	7.2000E+09	4.8000E+09	9.5000E+07	2.4400E+21
DIFFHEM	2.3800E+10	1.1100E+09	2.4000E-01	2.1100E+03	1.2000E+10	7.2000E+09	4.8000E+09	9.5000E+07	2.4400E+21
DIFFCAS2	2.3800E+10	1.1100E+09	2.4000E-01	2.1100E+03	1.2000E+10	7.2000E+09	4.8000E+09	9.5000E+07	2.4400E+21
DIFFCACL2	4.2300E+10	1.4000E+09	3.2400E-01	2.1500E+03	1.0000E+30	1.0000E+30	1.0000E+30	1.0000E+30	2.4400E+42
EMPTYDP	1.9000E+09	1.0000E+06	1.0000E-04	1.2200E+00	1.0000E+30	1.0000E+30	1.0000E+30	1.0000E+30	2.4400E+42

OFFSET	1.9000E+09	1.0000E+06	1.0000E-04	1.2200E+00	1.0000E+30	1.0000E+30	1.0000E+30	1.0000E+30	2.4400E+42